Crystal Structure of Human CD69: A C-Type Lectin-Like Activation Marker of Hematopoietic Cells[†,‡]

Kannan Natarajan,[§,||] Mark W. Sawicki,[||,⊥] David H. Margulies,*[,§] and Roy A. Mariuzza*[,⊥]

Molecular Biology Section, Laboratory of Immunology, National Institute of Allergy and Infectious Diseases, National Institutes of Health, Bethesda, Maryland 20892, and Center for Advanced Research in Biotechnology, University of Maryland Biotechnology Institute, 9600 Gudelsky Drive, Rockville, Maryland 20850

Received August 2, 2000; Revised Manuscript Received September 18, 2000

ABSTRACT: CD69 is a widely expressed type II transmembrane glycoprotein related to the C-type animal lectins that exhibits regulated expression on a variety of cells of the hematopoietic lineage, including neutrophils, monocytes, T cells, B cells, natural killer (NK) cells, and platelets. Activation of T lymphocytes results in the induced expression of CD69 at the cell surface. In addition, cross-linking of CD69 by specific antibodies leads to the activation of cells bearing this receptor and to the induction of effector functions. However, the physiological ligand of CD69 is unknown. We report here the X-ray crystal structure of the extracellular C-type lectin-like domain (CTLD) of human CD69 at 2.27 Å resolution. Recombinant CD69 was expressed in bacterial inclusion bodies and folded in vitro. The protein, which exists as a disulfide-linked homodimer on the cell surface, crystallizes as a symmetrical dimer, similar to those formed by the related NK cell receptors Ly49A and CD94. The structure reveals conservation of the C-type lectin-like fold, including preservation of the two α-helical regions found in Ly49A and mannose-binding protein (MBP). However, only one of the nine residues coordinated to Ca^{2+} in MBP is conserved in CD69 and no bound Ca^{2+} is evident in the crystal structure. Surprisingly, electron density suggestive of a puckered six-membered ring was discovered at a site structurally analogous to the ligand-binding sites of MBP and Ly49A. This sugar-like density may represent, or mimic, part of the natural ligand recognized by CD69.

The activation of lymphocytes triggers a series of biochemical and cellular events that ultimately lead to the regulated expression of a constellation of proteins, both intracellularly and at the cell surface. A formidable challenge in contemporary immunology is to delineate the functions and interrelationships of these proteins and thereby explain cellular function. One of the earliest cell surface molecules to appear following lymphocyte activation is CD69, known alternatively as early activation antigen (EA-1) (*1*), MLR-3 (*2*), activation inducer molecule (AIM) (*3*), or Leu-23 (*4*). CD69 is a disulfide-linked homodimer (*5*) expressed on a variety of hematopoietic cell surfaces including those of T, B, and natural killer (NK)[1] cells, monocytes, neutrophils, and platelets (*6*, *7*). Signals that trigger CD69 expression on lymphocytes include thymic maturation events (*8*), mitogenic or anti-CD3 stimulation of T cells (*4*), cross-linking of surface immunoglobulin on B cells (*9*), and cytokine (*4*), anti-CD16 (*10*), or anti-CD2 stimulation of NK cells (*11*). The functional effects of cross-linking cell surface CD69 with antibodies suggest a role for CD69 as a costimulatory molecule. In the presence of phorbol esters that activate the protein kinase C pathway, CD69 cross-linking on lymphocytes stimulates proliferation, cytokine secretion, Ca^{2+} mobilization, and cytotoxic responses (*3*, *12*, *13*). The cross-linking of CD69 expressed on monocytes (*14*), neutrophils (*15*), and platelets (*16*) leads to nitric oxide release, degranulation, and aggregation, respectively. Due to its strong correlation with other measures of lymphocyte activation, CD69 expression has been used widely to monitor the activation status of lymphocytes in inflammatory infiltrates. CD69 expression is elevated in T and NK cells infiltrating tumors (*17*), in lymphocytes from synovial tissue in rheumatoid arthritis (*18*), and in eosinophils from bronchial lavage in asthma (*19*).

The molecular cloning and nucleotide sequence determination of the CD69 gene from both human and mouse (*20*−*22*) has shown that the encoded molecule is a type II transmembrane protein that shares amino acid sequence homology with C-type animal lectins such as mannose-binding protein (MBP) and the selectins (*23*, *24*). Other members of this group include the NKR-P, Ly49, and NKG2/CD94 families of receptors, which are expressed predominantly on NK cells (*23*). As in other C-type lectin-like proteins, the putative carbohydrate recognition domain (CRD) of CD69 is encoded by three exons distinct from those

[†] This work was supported by NIH Grant AI47990. M.W.S is a recipient of a postdoctoral training fellowship from the Cancer Research Institute.

[‡] Atomic coordinates have been deposited in the Protein Data Bank as entry 1fm5.

* To whom correspondence should be addressed. (R.A.M.) Phone: (301) 738-6243. Fax: (301) 738-6255. E-mail: mariuzza@carb.nist.gov. (D.H.M.) Phone: (301) 496-6429. Fax: (301) 496-0222. E-mail: dhm@nih.gov.

[§] National Institutes of Health.

[||] These authors contributed equally to this work.

[⊥] University of Maryland Biotechnology Institute.

[1] Abbreviations: NK, natural killer; CRD, carbohydrate recognition domain; CTLD, C-type lectin-like domain; MBP, mannose-binding protein.

10.1021/bi0018180 CCC: $19.00
Published on Web 11/05/2000

encoding the cytoplasmic and transmembrane segments. However, the stem region, which connects the transmembrane domain to the CRD, is truncated in CD69. The gene encoding CD69 is present in a single copy and maps to human chromosome 12 and syntenic mouse chromosome 6. In the mouse, other C-type lectin-like NK receptors (NKR-P, NKG2/CD94, Ly49) map to the same region, designated the NK gene complex (*25*).

Despite its widespread distribution and intriguing expression pattern, the precise function of CD69 in hematopoietic and immune function remains unknown and awaits the identification of its physiological ligand(s). Surprisingly, recent studies on CD69 knockout mice failed to identify a dramatic effect on immunity (*26*). The development and function of T and NK cells, macrophages, granulocytes, and platelets in these animals appeared unaffected by the lack of CD69 expression. However, CD69 knockout mice displayed a small, but significant, increase in the steady-state number of bone marrow pre-B cells and in levels of serum IgM and IgG2a following immunization. The lack of a dramatic phenotype in CD69 knockout animals does not preclude an important function that might only be illustrated under extreme conditions. Frequently, knockout animals display only a subtle phenotype, even for profoundly important biological functions, unless they are appropriately stressed either genetically or physiologically (*27*−*29*).

To further our understanding of CD69 function and evolution, we have expressed a soluble form of the extracellular ligand-binding domain of human CD69 and determined its three-dimensional structure to 2.27 Å resolution. The structure reveals that CD69 adopts a fold similar to that of the CRD of C-type animal lectins (*23*, *24*). However, like the C-type lectin-like domains (CTLDs) of CD94 (*30*) and Ly49A (*31*), CD69 appears to lack the conserved Ca^{2+}-binding sites found in true C-type lectins. Unexpectedly, we observe electron density in the putative ligand-binding site of CD69 that could represent a possible ligand for this broadly distributed hematopoietic cell receptor.

EXPERIMENTAL PROCEDURES

Production of Recombinant CD69. A plasmid encoding human CD69 (*20*) was kindly provided by Dr. Steven Ziegler (Virgina Mason Research Center, Seattle, WA). Following PCR amplification and introduction of cloning sites, a fragment encoding the extracellular region, corresponding to amino acid residues 64−199, was directionally cloned into the *Nhe*I and *Bam*HI sites of pET21a (Novagen, Madison, WI), which added three amino acids (MetAlaSer) preceding Gly64. Protein was expressed in *Escherichia coli* BL21(DE3) cells from which inclusion bodies were prepared following lysozyme treatment, sonication, and extensive washing with 0.1% deoxycholate in 100 mM Tris-HCl, 2 mM EDTA, pH 8.0. Following solubilization in 6 M guanidine-HCl/0.1 mM DTT, the protein was folded without further purification by dilution into 0.4 M arginine, pH 9.5, containing 5 and 0.5 mM of reduced and oxidized glutathione, respectively. The folding mixture was dialyzed into 50 mM glycine, pH 9.5, concentrated, and applied to a Superdex 75 FPLC column (Pharmacia, Uppsala, Sweden) to separate protein aggregates from folded CD69. Further purification was carried out on a MonoS cation exchange column (Pharmacia) developed with a linear gradient of 0 to 0.5 M NaCl in 25 mM HEPES, pH 7.0. The purified soluble protein bound specifically to a monoclonal anti-human CD69 antibody, FN50 (Pharmingen, San Diego, CA), as detected by surface plasmon resonance using a Pharmacia BIAcore biosensor (data not shown).

Table 1: Data Collection and Refinement Statistics[a]

Data Collection	
data processing (room temperature, rotating anode)	
total observations to 2.90 Å	22 119
unique reflections	4072
completeness (%)	98.1 (97.7)
$I/\sigma I$	17.5 (4.6)
R_{sym}[b] (%)	11.0 (49.0)
data processing (flash frozen, argonne)	
total observations to 2.27 Å	36 807
unique reflections	13 674
completeness (%)	96.3 (86.5)
$I/\sigma I$	17.3 (2.3)
R_{sym}[b] (%)	6.2 (30.6)
Refinement	
data range	50.0−2.27 Å
no. of solvent atoms	137
rmsd bond lengths (Å)	0.0069
rmsd bond angles (deg)	1.38
rmsd dihedrals (deg)	22.76
rmsd impropers (Å)	0.76
R_{crys} (2σ cutoff)[c] (%)	24.31 (28.84)
R_{free} (2σ cutoff)[d] (%)	29.93 (30.92)
Ramachandran plot statistics	
most favored (%)	92.3
additional allowed (%)	7.7
disallowed (%)	0.0

[a] Values in parentheses indicate the value in the highest resolution shell (2.97−2.90 Å, rotating anode; 2.35−2.27 Å, argonne). [b] $R_{sym} = \sum|I_j - \langle I\rangle|/\sum I_j$, where I_j is the intensity of an individual reflection, and $\langle I\rangle$ is the average intensity of that reflection. [c] $R_{crys} = \sum||F_o| - |F_c||/\sum|F_o|$, where F_c is the calculated structure factor. [d] R_{free} is as for R_{crys} but calculated for a randomly chosen 5% of reflections that were omitted from the refinement.

Crystallization and Data Collection. Recombinant CD69 was crystallized by the hanging drop vapor diffusion method at 4 °C by mixing 1 μL of protein at a concentration of 7 mg/mL in 10 mM HEPES, 100 mM NaCl, pH 7.0, with 1 μL of reservoir solution containing 0.1 M sodium acetate, pH 4.5, 0.2 M zinc acetate, and 20% poly(ethylene glycol) 1000 (Wizard I Crystallization Screen, Emerald BioStructures, Bainbridge Island, WA). Two X-ray diffraction data sets were collected on the same CD69 crystal. Initially, data to 2.90 Å resolution were measured in-house at room temperature using a 345 mm MarResearch image plate detector with the crystal mounted in a capillary. The crystal belongs to space group $P3_121$, with $a = 49.1$ Å, $b = 49.1$ Å, $c = 122.0$ Å, $\alpha = \beta = 90.0°$, and $\gamma = 120.0°$. These cell dimensions are compatible with one CD69 monomer in the asymmetric unit. The crystal was extracted from the capillary and transferred to a modified mother liquor containing 20% ethylene glycol for cryogenic data collection on beamline 19D at the Advanced Photon Source, Argonne National Laboratory. The crystal was flash-frozen in liquid nitrogen and data were collected to 2.27 Å resolution. The cell dimensions were slightly altered: $a = 48.2$ Å, $b = 48.2$ Å, $c = 117.9$ Å, $\alpha = \beta = 90.0°$, and $\gamma = 120°$. The data were processed using the HKL2000 package (*32*).

Structure Determination. The structure was first determined to 2.90 Å resolution by molecular replacement

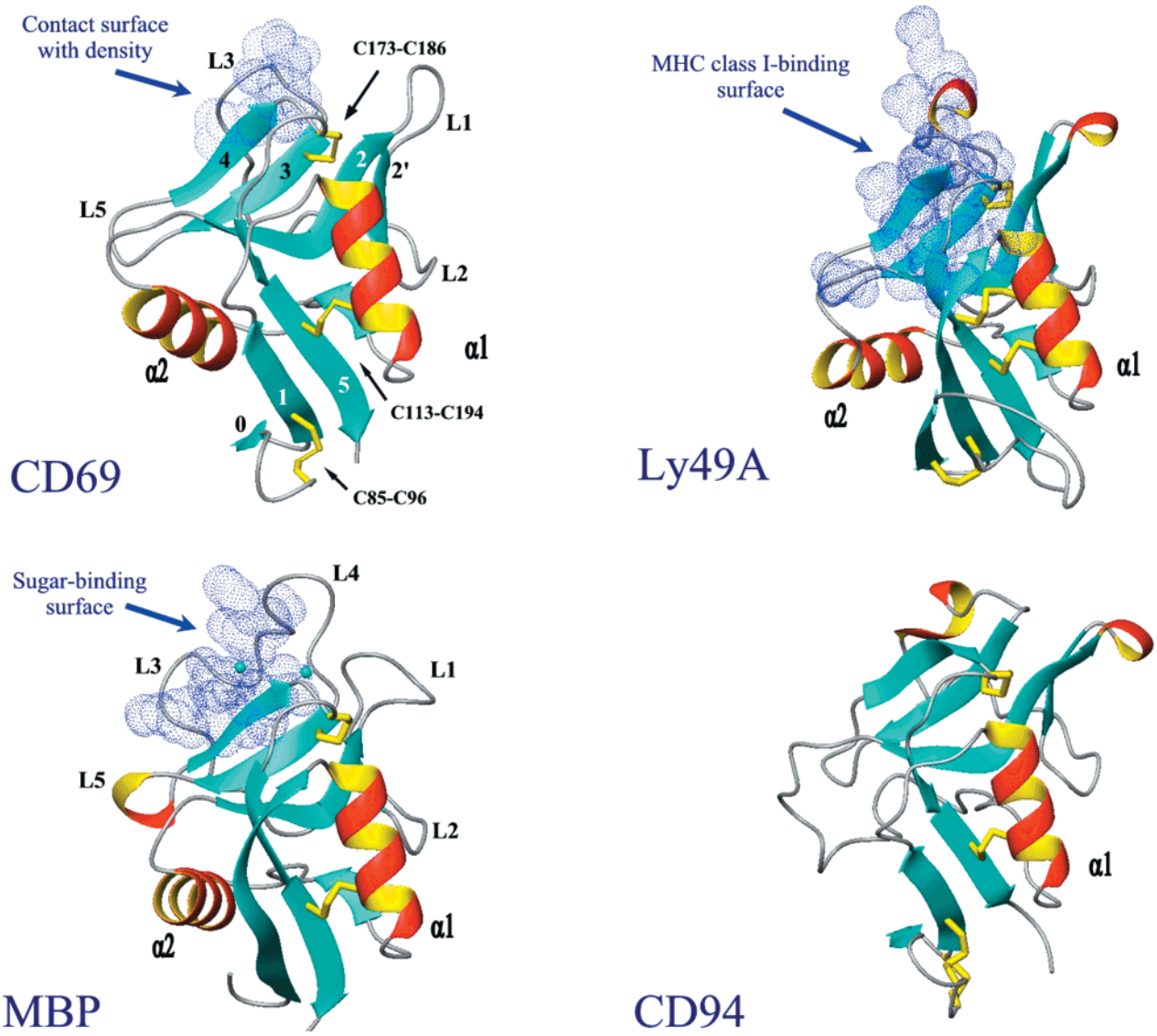

FIGURE 1: Ribbon diagrams of CD69, MBP-A, Ly49A, and CD94. β-Strands are blue, α-helices are red and yellow, and loop regions are shown as silver rope. The Ca^{2+} ions bound to MBP-A are drawn as blue spheres. The disulfide bonds are shown in yellow ball-and-stick representation. Secondary structure elements are labeled using the numbering for MBP-A (*36*). The surfaces shown in light blue illustrate the ligand-binding sites of MBP-A, and Ly49A, and the surface within van der Waals contact distance of the uncharacterized electron density in the CD69 structure. Figures 1 and 2 were generated using the program MOLMOL (*42*).

methods. A composite model constructed from the crystal structures of CD94 (PDB accession code 1B6E) and Ly49A (PDB accession code 1QO3) was used for the rotation and translation searches in AMoRe (*33*). The search yielded an unambiguous solution for the rotational (R = 52.2%, correlation coefficient = 29.0) and translational (R = 41.3%, correlation coefficient = 53.0) parameters, which resulted in an initial R_{crys} of 34.7%, and a correlation coefficient of 68.4 before rigid body refinement.

Crystallographic refinement was performed using CNS (*34*) utilizing simulated annealing refinement, bulk solvent correction, and individual temperature factor (B) refinement, alternating with iterative rounds of manual rebuilding in XtalView (*35*). Initial cycles of refinement were carried out using the 2.90 Å resolution room-temperature data. The final cycles of refinement were performed using the low-temperature synchrotron data to 2.27 Å. The current refined atomic model of CD69 is comprised of residues Ser78 to Ser80, Cys85 to Tyr198, and 137 water molecules. The final R_{crys} is 24.6%, and R_{free} is 29.7% for all data to 2.27 Å with $I > 2\sigma$. For the nonglycine residues, 92.3% fall in the most favored regions of the Ramachandran plot and none in the disallowed regions. Data collection and refinement statistics are shown in Table 1.

RESULTS AND DISCUSSION

CD69 Fold. The overall structure of CD69 is consistent with that of the CRDs of C-type animal lectins such as MBP (*23*, *36*), and the CTLDs of CD94 (*30*) and Ly49A (*31*). The molecule consists of two α-helices (α1 and α2) and two antiparallel β-sheets, and exhibits structural characteristics of both Ly49A and CD94 (Figure 1). The two β-sheets are formed by β-strands β0, β1 and β5, and β-strands β2, β2′, β3, and β4, respectively. This configuration of β-strands is similar to that observed in CD94 (*30*) and Ly49A (*31*), as evidenced by root-mean-square (rms) deviations of 1.35 and 1.31 Å, respectively, for the superposition of the α-carbon atoms of the 53 residues comprising the two β-sheets. The

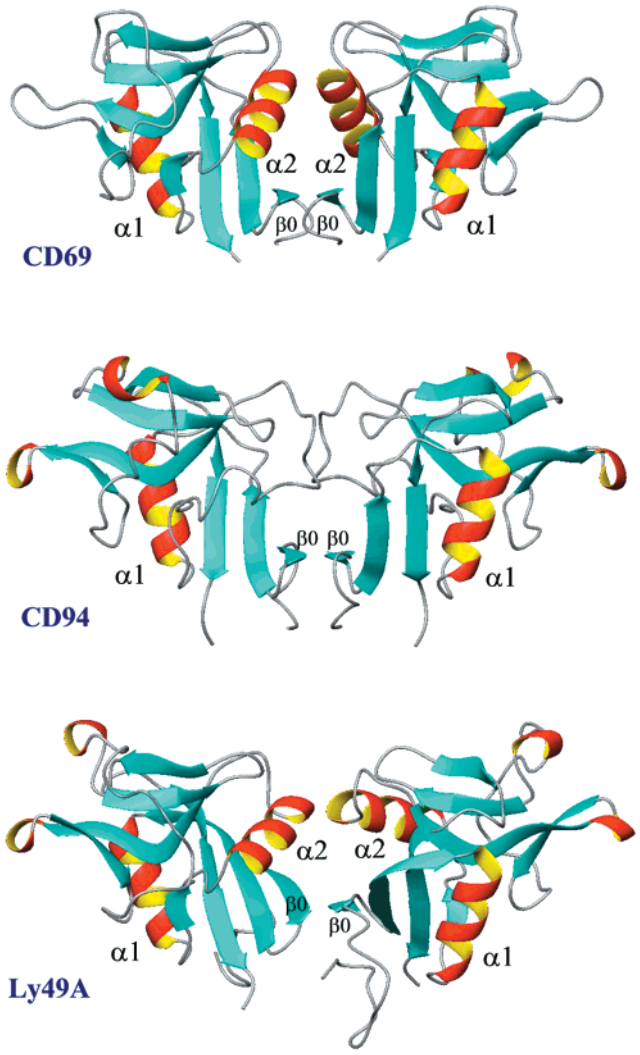

FIGURE 2: Ribbon models showing the CD69 dimer in comparison to the CD94 and Ly49A dimers. β-Strands are blue and α-helices are red and yellow. The secondary structure elements involved in dimer formation are labeled.

core β-sheets used for the superposition were derived from the Ly49A (*31*) structure since they are, on average, longer than those found in the CD69 structure. The β-strand configuration of CD69 is also similar to that of rat MBP (*36*), for which the rms deviation in α-carbon positions is 1.37 Å for 53 residues superimposed. However, the structure of CD69 includes strand β0, a characteristic of long-form CRDs (*37*), which is lacking in MBP (Figure 1). This β-strand is also present in CD94 and Ly49A, and is involved in noncovalent dimerization in all three structures (Figure 2). In CD69, β0 is three residues in length as in CD94, whereas in Ly49A this β-strand is six residues long. Despite these differences in length, all three CTLDs dimerize through β0 in a similar manner (Figure 2).

CD69 displays a number of significant structural differences compared to both CD94 and Ly49A. The most apparent of these involves the second helix, α2 (Figure 1). This helix is not present in CD94, where the corresponding residues adopt an extended loop structure (*30*). However, since the biologically functional form of CD94 is a heterodimer with NKG2 (*25*), it is unclear whether the absence of this helix in CD94 reflects the nonbiological CD94 homodimer that crystallized or represents a bona fide feature of the CD94/NKG2 heterodimer. Like CD69, Ly49A does have helix α2, although the orientation of the helix varies at the N-terminal end where it turns away from the central β-sheet (Figure 1). This difference appears to be due to the insertion of three residues at the N-terminal end of β0 in Ly49A, creating steric hindrance and forcing a repositioning of the α2 helix.

There are three intrachain disulfide bonds in the CD69 CTLD, Cys85−Cys96, Cys113−Cys194, and Cys173−Cys186, the latter two being the invariant disulfides found in all C-type animal lectins (Figures1 and 3). This is in contrast to the Ly49A and CD94 CTLDs, which have four intrachain disulfide bonds, two of them conserved. CD69 has an additional cysteine (Cys68), located within the stem region, which is not visible in the crystal structure. Although the in-vitro-folded molecule contains this residue, it does not form a covalent disulfide-linked dimer as assessed by SDS−PAGE under nonreducing conditions. Nevertheless, this cysteine could be involved in interchain disulfide bridging between CD69 monomers at the cell surface. The stem region, which includes residues Gly64 to Val82 in the crystallized recombinant protein, is largely disordered in the structure, except for three residues (Ser78, Asp79, and Ser80) wedged between two symmetry-related molecules. The fact that most of the stem is not visible implies that it is flexible, a feature which may enable the membrane-tethered CD69 CTLD to more easily engage its ligand(s).

As expected, based on the sequence homology in this region (Figure 3), loops 1 (residues 148−152) and 2 (residues 158−162) of CD69 are similar in structure to the corresponding loops of both Ly49A and CD94 (Figure 1). The conformation of loop 5 (177−180) follows that of Ly49A and MBP, but differs from that of loop 5 of CD94. This is because CD94 lacks helix α2 and the extended loop that replaces it forces loop 5 of CD94 to deviate from the conserved position of the loop seen in the other structures. CD69 also differs significantly from MBP-A with respect to loops 3 and 4 of the latter, which mediate Ca^{2+} and sugar binding in lectin members of the superfamily. Loop 3 of CD69 (residues 169−171) is shorter than the corresponding loops of MBP (loops 3 and 4; residues 184−193) and Ly49A (loop 3; residues 225−230) (Figure 3). This truncation causes the loop to adopt a tight, compact turn (Figure 1). Like Ly49A and CD94, CD69 probably lacks any Ca^{2+}-binding capacity as only one of four residues (Asp188 of rat MBP) coordinated to the first Ca^{2+} in MBP is conserved in CD69 (Asp171) (Figure 3) and no bound Ca^{2+} is observed in the crystal structure. Despite this, several residues responsible for saccharide recognition in MBP are present, as discussed below. Thus, the ability of CD69 to bind carbohydrate ligands is not necessarily precluded by its truncated loop 3. The second Ca^{2+}-binding site of MBP consists of five residues coordinating with the Ca^{2+} (*36*), none of which are conserved in the CD69 structure (Figure 3). In fact, the architecture of the second Ca^{2+}-binding site is dominated by contributions from loop 4, which the CD69 structure lacks.

CD69 Homodimer. At the cell surface, CD69 is a disulfide-linked homodimer (*5*), believed to be stabilized by an interchain disulfide bond between paired cysteines within the stem region (*6*). A 2-fold crystallographic dimer is observed in the crystal structure in which the monomers interact through their first β-strand, β0, creating one extended

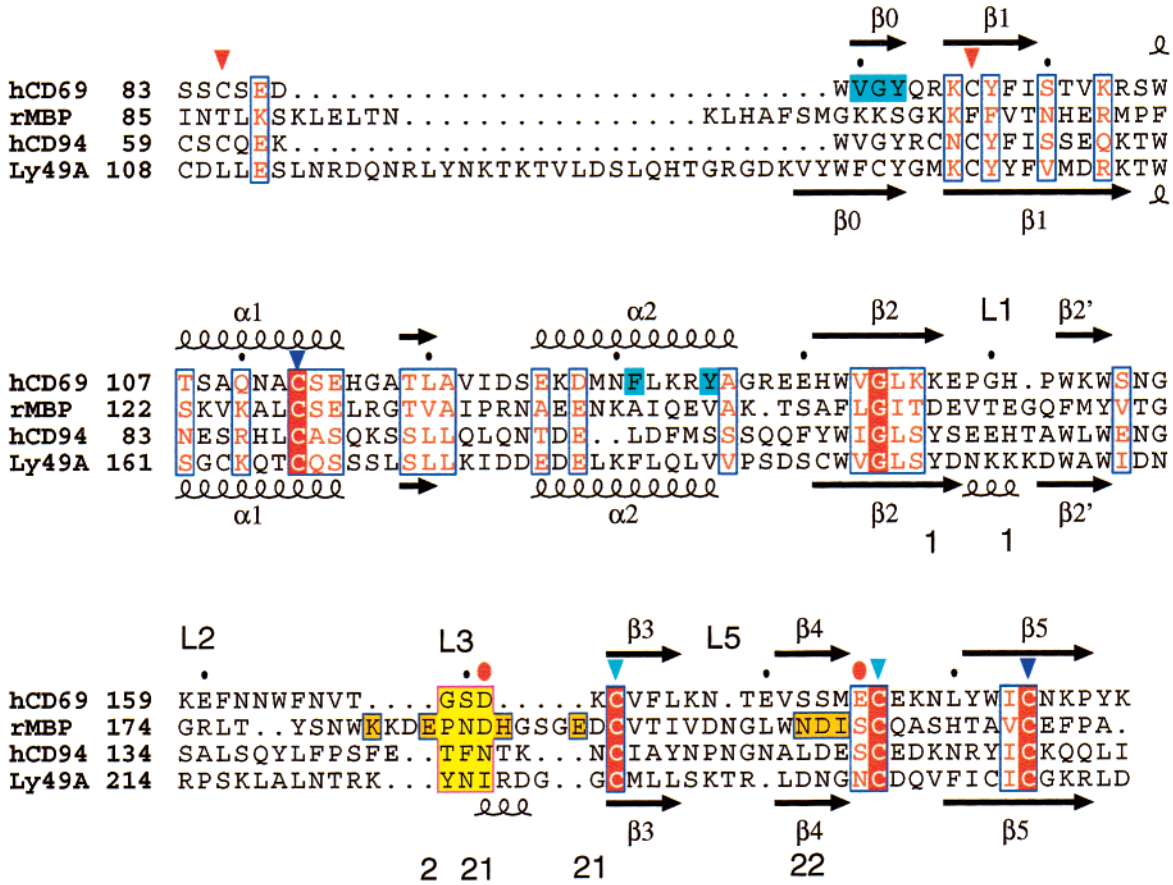

FIGURE 3: Structure-based alignment of human CD69 as compared with three other members of the C-type lectin-like family. On the basis of the three-dimensional structures of rat MBP-A (1msb), human CD94 (1b6e), and murine Ly49A (1qo3), the structures were superimposed to generate the indicated alignment which was visualized with ESPript 1.9 (http://www-pgm1.ipbs.fr:8080/ESPript, last accessed on August 1, 2000) written by P. Gouet and F. Metoz (*43*). Similarities were determined by the Risler matrix (*44*). Displayed amino acid residues are numbered. Secondary structure elements are displayed above for CD69 and below for Ly49A. Loop regions are numbered by analogy to the designation made for MBP-A (*36*). The residues of MBP-A that bind the two Ca^{2+} ions are indicated by numerals 1 and 2 below the alignment. Cysteines of CD69 involved in intrachain disulfide bonds are indicated by color-coded triangles. Residues involved in the hydrophobic dimer interface of CD69 are highlighted in cyan. Residues Asp171 and Glu185 of CD69 that appear to contact the uncharacterized electron density in the putative ligand-binding site are indicated by red circles. Residues of MBP-A that contact carbohydrate are highlighted in blue-bordered gold. The structurally similar loops of CD69, MBP-A, CD94, and Ly49A, corresponding to loop 3 of CD69, are highlighted in yellow.

Table 2: Interactions within the CD69 Dimer Interface

subunit 1	subunit 2	distance (Å)
hydrogen bonds		
Ser 87 O	Gln 93 N	2.89
Asp 88 Oδ2	Gln 93 Nε2	2.84
Gly 91 N	Gly 91 O	2.71
Asp 100 Oδ2	Lys 115 O	2.66
Arg 134 Nη2	Ala 136 O	2.80
Tyr 135 O	Arg 134 Nη1	3.28
hydrophobic interactions		
Tyr 135 Cδ1	Tyr 135 Cδ1	2.83
Val 90 Cγ2	Phe 131 Cε1	4.15
Val 90 Cγ2	Tyr 92 Cδ1	3.99
Val 90 Cγ1	Val 90 Cγ1	3.42
Tyr 135 Cε1	Phe 131 Cδ1	3.36

antiparallel β-sheet, and through helix α2 (Figure 2). The interface includes both hydrogen bonds and hydrophobic interactions (Table 2).

The portion of the dimer interface formed by the β0 stands is relatively flat with two main chain−main chain and two side chain−side chain hydrogen bonds between the strands (Figure 4A). In addition, the interface includes a central hydrophobic core formed by residues Val90, Gly91 and Tyr92 from β0, and Phe131 and Tyr135 from helix α2. In particular, Phe131 and Tyr135 pack against one another, forming a tight hydrophobic cluster at the C-terminal end of α2 (Figure 4B). Loop 5 shifts relative to its position in CD94 to allow for these packing interactions.

If one compares the CD94 and Ly49A homodimers to that of CD69, significant similarities are evident at the interfaces between monomers (Figure 2). All three CTLDs have a primary interface formed by strand β0 pairing with itself. The dimer arrangement in CD69 closely resembles that found in the CD94 crystallographic dimer, even though helix α2 has been replaced by a loop in the latter (*30*). This is reflected by most of the residues responsible for the tight hydrophobic interface in CD69, in particular Val90, Gly91, Tyr92, and Ile99, being identical to those involved in the formation of the hydrophobic interface in CD94 (Figure 3). In addition, the C-terminal ends of helix α2 pack against one another, forming a hydrophobic core, which is also found in the Ly49A structure. However, the angle between the two α2 helices in the CD69 dimer interface is smaller than in the Ly49A interface (145° compared to 170°), where the helices are more extended (Figure 2). The surface area buried at

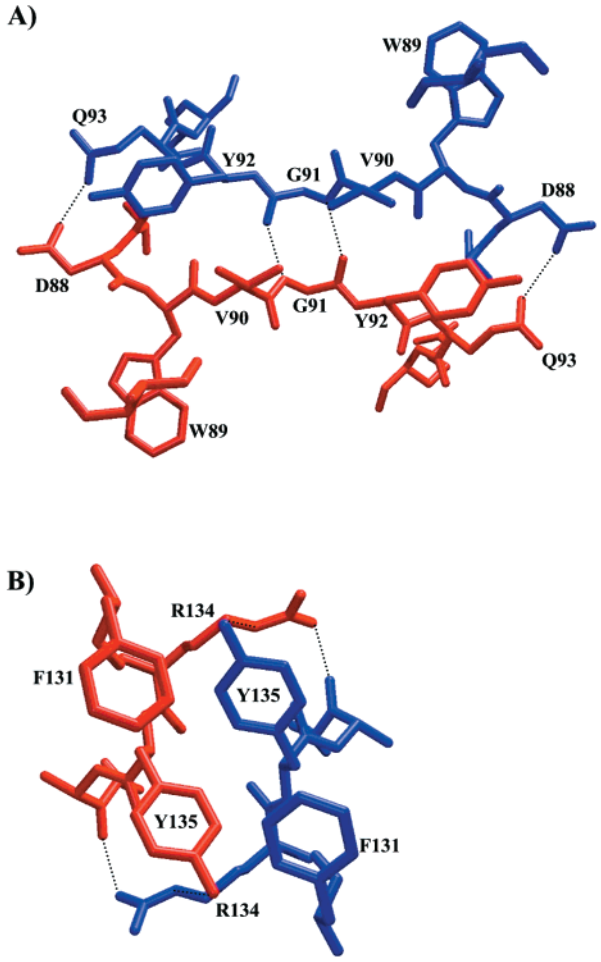

FIGURE 4: Ball-and-stick representations of the dimer interface of CD69. The two monomers composing the symmetrical homodimer are illustrated in red and blue. Hydrogen bonds are drawn as black dotted lines. All residues are labeled. (A) Hydrogen bonding between antiparallel β0 strands in the dimer interface. (B) Hydrophobic cluster formed by the α2 helices. The tight packing of the aromatic side chains of Phe131 and Tyr135 is evident. Figures 4 and 5 were generated using the program VMD (*45*).

the CD69 dimer interface is 1223 Å^2, nearly the same as that in the CD94 dimer (1204 Å^2), but larger than in Ly49A (931 Å^2). In the CD69 structure, as in Ly49A and CD94, the apposition of the two monomers generates a relatively flat, contiguous surface which is distal to both the N- and C-termini. The potential ligand-binding regions are at opposite ends of the flat surface, such that the CD69 dimer should be capable of bivalent binding (Figure 2).

Putative CD69 Ligand-Binding Site. Although a physiological ligand for CD69 is presently unknown, it is of interest to examine the region of this molecule, extending from loop 3 (residues 169−171) to β-strand 4 (residues 181−184), that corresponds to the ligand-binding site of other molecules of this family, in particular MBP and Ly49A, which bind saccharides and MHC class I proteins, respectively. This region of CD69 is nine residues shorter overall than the corresponding region of MBP, but a considerable portion of its backbone can be superimposed onto that of the other structure (Figure 5). It is provocative that here we observe extra electron density in the annealed omit map of CD69 ($F_o - F_c$) that cannot be accounted for by the amino acid sequence of the protein (Figure 6). Residues Asp171 and Glu185, located in this putative ligand-binding site, appear to contact the extra density. In addition, upon examination of the site on Ly49A that may interact with N-linked sugars on MHC class I (*31*), residues of CD69 that are comparable to those of Asp229 and Asn244 of Ly49A might also be available to interact with carbohydrate. Figure 1 compares the surface involved in ligand binding in the MBP (*36*) and Ly49A (*31*) structures to the surface that is within van der Waals distance of the electron density in the putative ligand-binding site of CD69. From this comparison, it is apparent that the same general region is implicated in all three proteins, suggesting that the extra density observed in the CD69 structure may indeed be located in the physiological ligand-binding site of this CTLD.

At this point, we have not been able to identify the molecule present within the CD69 CTLD. The density does not appear to be an ion or a component of the crystallization buffer. It is not an artifact of the cryogenic freezing since it is observed in the room-temperature structure as well. Unidentified electron density representing putative ligands has been observed in other structures, including HLA-A2 (*38*), CD1 (*39*), and isocitrate lyase (*40*), in which it was later shown that the unknown density corresponded to a physiological or a mimetic ligand. The density located within the putative ligand-binding site of CD69 has characteristics of a puckered six-membered ring similar to that of a hexose (Figure 6). However, the origin of such a ligand is not

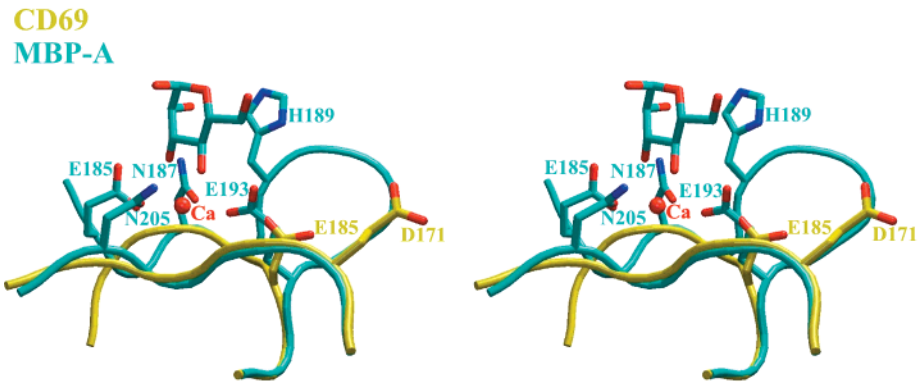

FIGURE 5: Superposition (in stereo) of the carbohydrate-binding site of MBP-A (blue) onto the putative ligand-binding site of CD69 (yellow). The side chains of MBP-A involved in mannose binding are labeled; the sugar is colored blue. The Ca^{2+} ion that coordinates mannose is drawn as a red sphere. Residues Asp171 and Glu185 of CD69, which are within van der Waals contact distance of the uncharacterized electron density, are shown.

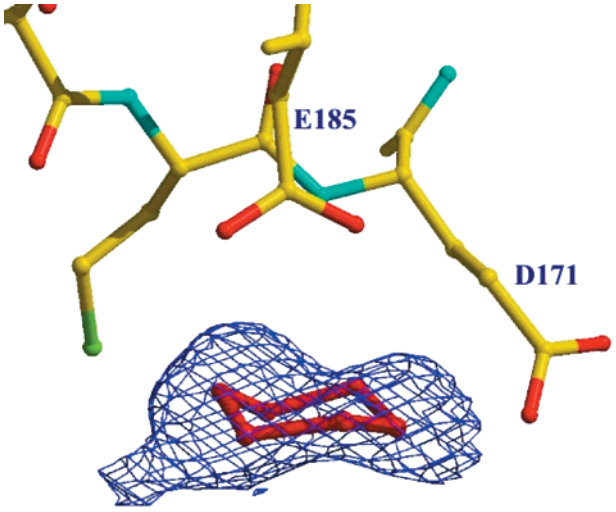

FIGURE 6: $F_o - F_c$ difference density found within the putative ligand-binding site of CD69, contoured at 2.9σ. A hexose has been placed arbitrarily within the electron density in order to illustrate the possibility that the density may correspond to a bound saccharide. The two residues (Asp171 and Glu185) within van der Waals distance of the density are labeled. This figure was generated using XtalView (*35*).

obvious, since the recombinant CD69 used in this study was folded in vitro from partially purified inclusion bodies, rather than in vivo by the bacterial host, where the folded protein could have fortuitously bound a component of *E. coli* that resembles its natural ligand(s). It should be noted, however, that the inclusion bodies were prepared simply by centrifugation and washing (see Materials and Methods) and, even though >90% pure on SDS−PAGE, may contain significant amounts of nonprotein contaminants (e.g. lipids, nucleic acids, polysaccharides). Thus, it is conceivable that CD69, once folded, could have bound a saccharide released from the bacterial cell wall by lysozyme treatment and carried over in the inclusion body preparation. However, a rigorous assessment of this (or any other) possibility must await the definitive identification of the bound molecule we observe in the CD69 crystal structure by microanalytical methods.

Conclusions. The three-dimensional structure of CD69, a member of the C-type lectin-like family, reveals strong similarities to the closely related NK receptors CD94 and Ly49A, whose structures have recently been determined (*30*, *31*). This structural homology is clear despite the relatively weak amino acid sequence identity among the CTLDs of these three molecules (CD69 is 17% identical to CD94 and 23% identical to Ly49A). All three molecules display similar overall folds and core structures, are stabilized by conserved disulfide bonds, and dimerize through their β0 strands. The mode of dimerization is conserved through intrachain and interchain hydrogen bonding, and discrete conserved hydrophobic residues within β0. In addition, electron density has been observed within the putative-ligand binding site of CD69. Although the density cannot be defined with confidence at this time, the fact that it is proximate to amino acid residues that are conserved between CD69 and the MBP carbohydrate-binding site is suggestive that the density may in fact be a part of the natural ligand of CD69, or may be structurally related to it. Although the ligand for CD69 has not been identified, it may be another cell surface glycoprotein (*6*, *7*). This is the case for Ly49A and CD94/NKG2, which recognize the MHC class I molecules H-2D^d and HLA-E, respectively (*25*). Since no Ca^{2+} ions are present in the putative ligand-binding domain of CD69, and there is little conservation of residues that constitute the Ca^{2+}-binding sites of MBP, CD69 seems to represent a form divergent from the true C-type lectins. Ly49A, which binds its MHC class I ligand in the absence of Ca^{2+} (*31*, *41*), displays similar divergence. The intriguing discovery of sugar-like electron density in the crystal structure of CD69 opens promising new approaches to characterizing the ligand specificity of this enigmatic cell activation marker.

REFERENCES

1. Hara, T., Jung, L. K., Bjorndahl, J. M., and Fu, S. M. (1986) *J. Exp. Med. 164*, 1988−2005.
2. Cosulich, M. E., Rubartelli, A., Risso, A., Cozzolino, F., and Bargellesi, A. (1987) *Proc. Natl. Acad. Sci. U.S.A. 84*, 4205−4209.
3. Cebrian, M., Yague, E., Rincon, M., Lopez-Botet, M., de Landazuri, M. O., and Sanchez-Madrid, F. (1988) *J. Exp. Med. 168*, 1621−1637.
4. Lanier, L. L., and Phillips, J. H. (1988) *Ann. Inst. Pasteur Immunol. 139*, 450−456.
5. Sanchez-Mateos, P., and Sanchez-Madrid, F. (1991) *Eur. J. Immunol. 21*, 2317−2325.
6. Testi, R., D'Ambrosio, D., De Maria, R., and Santoni, A. (1994) *Immunol. Today 15*, 479−483.
7. Marzio, R., Mauel, J., and Betz-Corradin, S. (1999) *Immunopharmacol. Immunotoxicol. 21*, 565−582.
8. Vanhecke, D., Leclerq, G., Plum, J., and Vandekerchove, B. (1995) *J. Immunol. 155*, 1862−1872.
9. Rasmussen, A. M., Blomhoff, H. K., Stokke, T., Horejsi, V., and Smeland, E. B. (1994) *J. Immunol. 153*, 4997−5007.
10. Falini, B., Pileri, S., and Martelli, M. F. (1989) *Crit. Rev. Oncol. Hematol. 9*, 351−419.
11. Gerosa, F., Tommasi, M., Scardoni, M., Accolla, R. S., Pozzan, T., Libonati, M., Tridente, G., and Carra, G. (1991) *Mol. Immunol. 28*, 159−168.
12. Testi, R., Phillips, J. H., and Lanier, L. L. (1989) *J. Immunol. 143*, 1123−1128.
13. Moretta, A., Poggi, A., Pende, D., Tripodi, G., Oregno, A. M., Pella, N., Augugliaro, R., Bottino, C., Ciccone, E., and Moretta, L. (1991) *J. Exp. Med. 174*, 1393−1398.
14. De Maria, R., Cifone, M. G., Trotta, R., Rippo, M. R., Festuccia, C., Santoni, A., and Testi, R. (1994) *J. Exp. Med. 180*, 1999−2004.
15. Gavioli, R., Risso, A., Smilovich, D., Baldissarro, I., Capra, M. C., Bargellesi, A., and Cosulich, M. E. (1992) *Cell. Immunol. 142*, 186−196.
16. Testi, R., Pulcinelli, F., Frati, L., Gazzaniga, P. P., and Santoni, A. (1990) *J. Exp. Med. 172*, 701−707.
17. Van den Hove, L. E., Van Gool, S. W., Van Poppel, H., Baert, L., Coorevits, L., Van Damme, B., and Ceuppens, J. L. (1997) *Clin. Exp. Immunol. 109*, 501−509.
18. Iannone, F., Corrigal, V. M., and Panayi, G. S. (1996) *Br. J. Rheumatol. 35*, 397.
19. Hartnell, A., Robinson, D. S., Kay, A. B., and Wardlaw, A. J. (1993) *Immunology 80*, 281−286.
20. Ziegler, S. F., Ramsdell, F., Hjerrild, K. A., Armitage, R. J., Grabstein, K. H., Hennen, K. B., Farrah, T., Fanslow, W. C., Shevach, E. M., and Alderson, M. R. (1993) *Eur. J. Immunol. 23*, 1643−1648.
21. Hamann, J., Fiebig, H., and Strauss, M. (1993) *J. Immunol. 150*, 4920−4927.
22. Lopez-Cabrera, M., Santis, A. G., Fernandez-Ruiz, E., Blacher, R., Esch, F., Sanchez-Mateos, P., and Sanchez-Madrid, F. (1993) *J. Exp. Med. 178*, 537−47.
23. Weis, W. I., Taylor, M. E., and Drickamer, K. (1998) *Immunol. Rev. 163*, 19−34.
24. Drickamer, K. (1999) *Curr. Opin. Struct. Biol. 9*, 585−590.
25. Lanier, L. (1998) *Annu. Rev. Immunol. 16*, 359−393.

26. Lauzurica, P., Sancho, D., Torres, M., Albella, B., Marazuela, M., Merino, T., Bueren, J. A., Martinez-A, C., and Sanchez-Madrid, F. (2000) *Blood 95*, 2312−2320.
27. Koller, B. H., Marrack, P., Kappler, J. W., and Smithies, O. (1990) *Science 248*, 1227−1230.
28. Dong, C., Yang, D. D., Tournier, C., Whitmarsh, A. J., Xu, J., Davis, R. J., and Flavell, R. A. (2000) *Nature 405*, 91−94.
29. Egan, P. J., and Carding, S. R. (2000) *J. Exp. Med. 191*, 2145−2158.
30. Boyington, J. C., Riaz, A. N., Patamawenu, A., Coligan, J. E., Brooks, A. G., and Sun, P. D. (1999) *Immunity 10*, 75−82.
31. Tormo, J., Natarajan, K., Margulies, D. H., and Mariuzza, R. A. (1999) *Nature 402*, 623−631.
32. Otwinowski, Z., and Minor, W. (1997) *Methods Enzymol. 276*, 307−326.
33. Navaza, J. (1994) *Acta Crystallogr., Sect. A 50*, 157−163.
34. Brunger, A. T., Adams, P. D., Clore, G. M., DeLano, W. L., Gros, P., Grosse-Kunstleve, R. W., Jiang, J.-S., Kuszewski, J., Nilges, M., Pannu, N. S., Read, R. J., Rice, L. M., Simonson, T., and Warren, G. L. (1998) *Acta Crystallogr., Sect. D 54*, 905−921.
35. McRee, D. E. (1999) *J. Struct. Biol. 125*, 156−65.
36. Weis, W. I., Kahn, R., Fourme, R., Drickamer, K., and Hendrickson, W. A. (1991) *Science 254*, 1608−1615.
37. Day, A. J. (1994) *Biochem. Soc. Trans. 22*, 83−88.
38. Bjorkman, P. J., Saper, M. A., Samraoui, B., Bennett, W. S., Strominger, J. L., and Wiley, D. C. (1987) *Nature 329*, 506−512.
39. Zeng, Z., Castano, A. R., Segelke, B. W., Stura, E. A., Peterson, P. A., and Wilson, I. A. (1997) *Science 277*, 339−345.
40. Britton, K., Langridge, S., Baker, P., Weeradechapon, K., Sedelnikova, S., De Lucas, J., Rice, D., and Turner, G. (2000) *Structure 8*, 349−362.
41. Natarajan, K., Boyd, L. F., Schuck, P., Yokoyama, W. M., Eilat, D., and Margulies, D. H. (1999) *Immunity 11*, 591−601.
42. Koradi, R., Billeter, M., and Wüthrich, K. (1996) *J. Mol. Graphics 14*, 51−55.
43. Gouet, P., Courcelle, E., Stuart, D. I., and Metoz, F. (1999) *Bioinformatics 15*, 305−308.
44. Risler, J. L., Delorme, M. O., Delacroix, H., and Henaut, A. (1988) *J. Mol. Biol. 204*, 1019−1029.
45. Humphrey, W., Dalke, A., and Schulten, K. (1996) *J. Mol. Graphics 14*, 33−38.

BI0018180